Nonmonotonic Response of Primary Production and Export to Changes in Mixed-Layer Depth in the Southern Ocean

Joan Llort, Marina Lévy, Jean-Baptiste Sallée, Alessandro Tagliabue

Non-monotonic response of primary production and export to changes in mixed-layer depth in the Southern Ocean

J. Llort[1,2], M. Lévy[3], J.B.Sallée[3] and A.Tagliabue[4]

[1] Institute of Marine and Antarctic Studies, University of Tasmania, Hobart, Australia

[2] Australian Research Council Centre of Excellence for Climate System Science, Hobart, Tasmania, Australia

[3] Sorbonne Université, LOCEAN-IPSL, CNRS/IRD/MNHN, Paris, France

[4] School of Environmental Sciences, University of Liverpool, UK

Corresponding author: Joan Llort (jllort@utas.edu.au)

Key Points:

- Moderate shoaling of winter mixed layer causes increase in primary production but shoaling below a threshold depth can lead to a collapse.
- Reversal in this response is due to balancing effects of iron and light limitation and associated with a change in community structure and export efficiency.
- Interestingly, shoaling summer mixed layer always reduces PP and export because of a reduction of the productive volume.

Abstract

Ongoing and future changes in wind and temperature are predicted to alter upper ocean vertical mixing across the Southern Ocean. How these changes will affect primary production (PP) remains unclear as mixing influences the two controlling factors: light and iron. We used a large ensemble of 1D-biogeochemical model simulations to explore the impacts of changes in mixed-layer depths (MLD) on PP in the Southern Ocean. In summer, shoaling MLD always reduced depth-integrated PP, despite increasing production rates. In winter, shoaling mixed-layers had a two-staged impact: for moderate shoaling PP increased as light conditions improved, but more pronounced shoaling decreased iron supply, which reduced PP. The fraction of PP exported below 100m also presented a non-monotonic behavior. This suggests a potential future shift from a situation where reduced winter mixing increases PP and export, to a situation where PP and export may collapse if the ML shoals above a threshold depth.

Plain Language Summary

In the Southern Ocean, atmospheric warming associated to climate change is altering the depth at which surface waters are stirred, the so-called *mixed-layer depth*. A change in the *mixed-layer depth* impacts the phytoplankton cells that inhabit it by altering their two main limiting factors: iron and light. However, the sign and magnitude of this impact are still not clear. In this work we used mathematical simulations to explain how changes in the seasonal *mixed-layer depth* modify the supply of iron and the amount of light, and how these changes impact phytoplankton activity. Our results show that *mixed-layer depth* changes in summer and in winter have different impacts. Reducing summer *mixed-layer depth* did not change the iron supply but it reduced the volume of water where phytoplankton thrived. In winter, shallower *mixed-layer depth* altered iron and light but in opposed ways. At first, phytoplankton increased its activity as more light became available. However, a continued shallowing of the *mixed-layer depth* eventually reduced the iron supply and the phytoplankton activity. Our study proposes a new interpretation on how ongoing changes in the Southern Ocean impact phytoplankton activity and alerts of the presence of threshold depths for the winter mixed-layer above which phytoplankton may struggle to survive.

1 Introduction

Southern Ocean (SO) atmospheric and oceanic conditions are currently changing in response to increasing atmospheric concentrations of greenhouse gases and changes in the concentration of stratospheric ozone (Swart et al, 2018). Model projections from the fifth phase of the Coupled Model Intercomparison Project (CMIP5, Taylor et al., 2012) highlight a changing wind pattern associated with a more persistent phase of the Southern Annular Mode (SAM), together with warmer sea-surface temperature north of the sea-ice zone (Bracegirdle et al., 2013; Cai et al, 2003; Swart et al, 2015; Zheng et al, 2013). Such changes in the physical environment are expected to affect the capacity of phytoplankton to fix atmospheric carbon, their community composition and the overall efficiency of the biological carbon pump (Lenton and Matear, 2007; Lovenduski and Gruber, 2005). In particular, it is critical to understand how physical changes will alter iron and light availability, as these two elements play fundamental roles in structuring the response of phytoplankton communities (Boyd et al, 2002).

In a recent review, Deppeler and Davidson (2017) identified a large number of factors able to alter primary production in the Southern Ocean. Amongst these factors, changes in the seasonal mixed-layer depth (MLD) were particularly important north of the sea-ice zone. However, neither the sign nor the magnitude of change are yet clear due to the complex links between the seasonal cycle of the MLD and primary production in the Southern Ocean. Two reasons contribute to this complexity. First, the sign of the change in MLD is expected to vary regionally and seasonally, depending on changes in surface warming, wind and freshwater fluxes (Panassa et al, 2018, Sallée et al, 2013). Second, vertical mixing plays a complex role for phytoplankton, since shallow MLDs may maintain cells in the well-lit part of the water column, but, at the same time, the vertical extent of the upper mixing layer controls the vertical supply of iron from deeper reserves. Thus, while a decrease in MLD enhances productivity in light limited conditions through the first mechanism, it reduces productivity through the second mechanism in regions where iron is supplied by vertical mixing in winter (Doney, 2006; Sarmiento et al, 2004). In this second case, the winter supply of iron is more efficient when the mixed-layer deepens within the subsurface iron reservoir (hereafter, we refer to the upper limit of the iron reservoir as the ferricline, see methods for details). The two mechanisms described by this paradigm are concomitant in the Southern Ocean, where both light limitation and iron limitation co-exist in

time and space (Boyd et al 2010). Moreover, given that such interplay varies throughout the seasonal cycle, changes in the seasonal extremes of the MLD in winter and summer (MLD_{winter} and MLD_{summer}, respectively) are expected to have different impacts on annual values of primary production (Deppeler and Davidson, 2017, Hauck et al, 2015).

End-of-century projections from CMIP5 show a coherent latitudinal pattern of change in primary production over the Southern Ocean (Bopp et al, 2013; Laufkötter et al, 2015). In the 30°-40°S latitudinal band CMIP5 models agree on a nutrient-driven decrease in primary production as a consequence of the broadening of oligotrophic gyres to southern waters (Hauck et al, 2015). In the 40°-50°S latitudinal band, models project an increase in primary production, followed by a decrease in the 50°-65°S band (Bopp et al 2013). Leung et al. (2015) found a consistent response between models on the primary production increase at 40°-50°S. Their analysis associated the change in primary production to a reduction of MLD_{summer} combined with an increase in surface iron. Alternatively, the primary production decrease in the 50°-65°S band was not consistent between models and has been linked to deeper MLD_{summer} combined with a reduction of the incident photosynthetically available radiation. However, the mechanisms behind these changes remain unclear as projected patterns have only been explained through correlation relationships (Leung et al, 2015), or masked by the strong primary production increase associated to Antarctic sea-ice decline (Laufkötter et al, 2015). The overlap between different drivers in climate models does not allow evaluating the influence of changes in MLD alone over primary production. Furthermore, the uncertainties in these models are likely to induce incorrect interpretations based on theoretical paradigms (Lovenduski and Gruber, 2005). The largest uncertainty is caused by the inability of CMIP5 models to correctly reproduce dissolved iron and MLD observations in the Southern Ocean (Sallée et al, 2015; Tagliabue et al, 2016), particularly in winter. These uncertainties cascade into the iron vertical supply and cause a model-dependent biogeochemical response in the Southern Ocean (Schourup-Kristensen, 2014).

Moreover, the lack of mechanistic understanding and the uncertainties associated to primary production drivers in the Southern Ocean also impact the estimates of how much carbon is eventually transferred into the deep ocean. The export of carbon depends on a number of processes such as the plankton community structure, remineralization rates, temperature or MLD variability (Boyd and Trull, 2007; Henson et al, 2015). The disparities on how biogeochemical

models resolve these mechanisms add up to iron supply uncertainties and cause a lack of agreement between climate-models in the Southern Ocean (Laufkötter et al, 2016). This lack of consensus is particularly severe in the mid-latitudes, 44°-58°S (Hauck et al, 2015).

A number of observation-based studies provide evidences that in the Southern Ocean the two aspects of the primary production-MLD paradigm (Fig 1 in Doney, 2006) might be occurring simultaneously. Ardyna et al. (2017) combined data from satellite ocean-color with Argo floats to show that regional variability in Southern Ocean phytoplankton biomass results from a mixed balance of drivers in addition to light, including the proximity to island or submerged seamounts, sea-ice, or MLD_{winter}. Interestingly, they show that, away from specific iron sources, phytoplankton biomass increases as a function of MLD_{winter}, for MLD_{winter} ranging from 0 to ~150m, but decreases for MLD_{winter} > 150m. They interpret the presence of such a regime shift as a transition from an iron-limited environment (shallow MLD_{winter}) to a light-limited environment (deep MLD_{winter}). Similarly, Hoppe et al. (2017) reported strong blooming conditions in regions of deep mixing, suggesting a secondary role of light limitation on controlling summer production. This result agrees with Venables and Moore (2010) who found no influence of light limitation over the annual integrated chlorophyll-a in Southern Ocean waters.

In this paper, we investigate how ongoing and future changes in winter and summer MLD may influence primary production and the export of organic carbon with a modeling configuration specifically designed to address this question in the context of the Southern Ocean. Our approach avoids the complexity related to climate models and, at the same time, captures the double-role of the MLD on primary production. To do so, we implemented a state-of-the-art biogeochemical model into a fully controlled one-dimensional (1D) physical configuration. We varied MLD_{winter}, MLD_{summer} and ferricline depth (Z_{Fe}) along typical present and projected ranges for the Southern Ocean. Despite the idealized approach, the statistical analysis of a large ensemble (752) of simulated annual cycles showed a complex relationship between MLD, primary production and export. Our results challenge current interpretations of CMIP5 projections in the Southern Ocean and propose the presence of a threshold depth for MLD_{winter} below which production would collapse.

2. Methods

Our model configuration represents an ocean water column resolved as a vertical grid of 75 equally spaced cells. Only vertical exchanges are considered (i.e., it is a 1D configuration). The same configuration was used in Llort et al. (2015) to study the bloom phenology in the SO and is fully described therein; here we recall the fundamental model characteristics. We use the biogeochemical model PISCES (Aumont and Bopp, 2006) that we force with three physical variables: surface solar short-wave radiation, temperature and turbulent vertical mixing (κ_z). These three variables are prescribed and follow a complete seasonal cycle starting on the 15th of February. The vertical profile of κ_z is set as a step-like function, with a value of 1 m^2 s^{-1} within an upper mixed-layer and a small open ocean mixing of 10^{-5} m^2 s^{-1} (Cisewski et al, 2005) below the mixed-layer. The strong mixing in the upper layer ensures a homogenous vertical distribution of phytoplankton and nutrients (Lévy, 2015). The depth of the surface mixed-layer (and thus the penetration depth of strong vertical mixing) varies along an idealized seasonal cycle consisting of three phases (Fig 1a,b): a first phase of linear deepening until the maximum depth (MLD_{winter}, from 15th February to 15th September), a second phase of linear shoaling (from 15th September to 15th December) and a period of constant depth in summer (MLD_{summer}, 15th December to 14th February of the next year).

PISCES contains 24 biogeochemical tracers, among which five nutrients (nitrate, phosphate, ammonium, iron, and silicate), two phytoplankton size classes (small and large) and two zooplankton size classes (micro-zooplankton and meso-zooplankton). Large phytoplankton differs from small phytoplankton by higher iron requirements and a greater iron half-saturation constant.

Initial vertical profiles for macronutrient (i.e. nitrate, phosphate, and silicate) were constructed based on the winter mean profiles of a typical HNLC region (Jeandel et al., 1998). We carried a series of sensitivity experiments to ensure that only iron limits phytoplankton growth. The summer initial condition for dissolved iron profile was constructed by assuming low concentrations (0.03 nmol Fe l^{-1}) above a prescribed depth and larger concentrations (0.5 nmol Fe l^{-1}) below. The depth where iron concentration suddenly increases is referred here as the ferricline (Z_{Fe}). Iron supply into the upper mixed layer is not prescribed, but emerges from the

vertical entrainment and diffusion of iron, which depends on the respective depth of the Z_{Fe} and the MLD. While lateral advection might be another important source of dissolved iron in specific SO regions, particularly in the lee of islands or continental shelves, it is neglected here to concentrate on vertical entrainment of iron. Vertical entrainment of iron is likely the dominant source of iron supply in most of the Southern Ocean, which is characterized by deep ferricline (Tagliabue et al., 2014). In this study, iron supply is computed as the amount of dissolved iron that enters MLD.

Ensemble of runs

The 1D physical setting forced the PISCES model under current and future MLD conditions. We conducted an ensemble of simulations where we varied three forcing parameters, MLD_{winter}, MLD_{summer} (Pellichero et al, 2017) and Z_{Fe} (Tagliabue et al, 2014), over the full range of observed values in the SO. Values for future MLD were obtained from CMIP5 climate model projections (Sallée et al, 2013; Taylor et al, 2012). Overall, we prescribed 11 distinct values of MLD_{winter} (between 100m and 600m), combined with 9 distinct values for MLD_{summer} (between 20m and 100m) and 8 Z_{Fe} values (between 150 and 500m). The combination of all MLD_{winter}, MLD_{summer} and Z_{Fe} values resulted in 752 different scenarios. This approach allowed us to identify how changes in MLD affect primary production and export over a wide range of oceanic conditions typical of the Southern Ocean.

4 Results

4.1 Response to changes in winter MLD

Southern Ocean open waters extend from mid to high-latitudes, with seasons being clearly differentiated and incident Photosynthetically Available Radiation (PAR) being lower in winter than in summer. However, the average light received by phytoplankton is lower than surface PAR as cells are vertically mixed across the mixed-layer. The light used for the photosynthesis can then be calculated using the PAR attenuation profile averaged across the mixed-layer (PAR_{ML}). Thus, deeper (shallower) MLD_{winter} reduce (increase) PAR_{ML}, exacerbating (relaxing) light limitation of phytoplankton growth and primary production (Boyd et al, 2010). MLD_{winter} also has an impact on growth and primary production limitation by controlling vertical supply of

194 iron. Deeper MLD_{winter} tend to drive stronger iron supplies and enhance phytoplankton growth
195 (Tagliabue et al, 2014). We first examine how the combination of these two opposing
196 mechanisms (light and iron limitation) drive differences in primary production in three model
197 simulations that only differ by their MLD_{winter} values (deep, intermediate and shallow scenario),
198 with identical MLD_{summer} and Z_{Fe} (Fig 1, left panels).

199 From March to July, the seasonal decrease of surface PAR combined with the deepening of the
200 mixed-layer strongly decreased PAR_{ML} for all three scenarios (Fig 1a and b). PAR_{ML} remained
201 low until October, when the shoaling of the MLD caused a rapid increase (Fig. 1b). The vertical
202 supply of iron initiated when the mixed-layer depth crossed Z_{Fe} (Fig 1b). These two factors,
203 PAR_{ML} and iron supply, acted together to shape the response in primary production (Fig 1c and
204 d). From March to July, depth-integrated primary production was low and with a decreasing
205 trend (Fig 1c). For the three scenarios a period of slow increase started around July, and was
206 followed by a marked bloom in spring.

207 The three simulations exhibited differences in the timing and amplitude of the bloom (Fig. 1c).
208 In the shallow simulation, winter iron supply was relatively low (24 μmolFe m^{-2} yr^{-1}) and the
209 bloom was the weakest and earliest. Production started increasing on July 1st and peaked in
210 November, shortly after the mixing layer started shoaling and a month after iron supply ceased
211 (Fig. 1a, b and c). On the contrary, the bloom in the deep MLD_{winter} simulation was the strongest
212 and the slowest to develop of all three scenarios. In this scenario, MLD_{winter} penetrated deeply
213 into Z_{Fe}, which enhanced the vertical flux of iron (60 μmolFe m^{-2} yr^{-1}). Nevertheless, integrated
214 primary production did not increase until the mixed-layer started shoaling in October. The large
215 amount of accumulated iron during winter and the quick spring increase in PAR_{ML} supported a
216 strong, but relatively short bloom, peaking in December.

217 Interestingly, these two extreme simulations led to similar values of annual integrated primary
218 production (74.8 gC m^{-2} yr^{-1} for the shallow simulation and 75.5gC m^{-2} yr^{-1} for the deep
219 simulation, Fig 1d), yet the relative contributions of small and large phytoplankton were notably
220 different. The annual primary production supported by the large phytoplankton group
221 represented 34% of the total production for the iron-poor shallow simulation while for the iron-
222 rich deep simulation it reached 52% (dashed lines in Fig 1d).

When these two end-members simulations are compared to the intermediate MLD_{winter} scenario a non-monotonic response of annual primary production to varying MLD_{winter} emerges. While the bloom in the intermediate MLD_{winter} simulation presented intermediate characteristics (iron supply was 53 μmolFe m^{-2} yr^{-1}, Fig 1c), it showed the highest annual production (79.1 gC m^{-2} yr^{-1}) of all three simulations (Fig 1d). The balance between a weak, long-lasting and small-phytoplankton-dominated winter bloom; and a high, quick and large-phytoplankton-dominated spring bloom appeared to be optimal in the case of the intermediate experiment.

When we analyzed the results from our ensemble of 752 simulations (Fig. 2a), two contrasted modes emerged in the response of annual primary production (PP) to changes in MLD_{winter}. The first mode was associated with a deep iron reservoir (Z_{Fe}>350 m), and the second mode with a shallow iron reservoir (Z_{Fe}<250 m). Both modes presented non-monotonic PP-MLD_{winter} relationships: for a given Z_{Fe}, PP increased as MLD_{winter} decreased, until MLD_{winter} reached a threshold depth ($Z_{PPmax,}$ indicated by the white contours in Fig. 2a), where the PP–MLD_{winter} relationship reversed and PP started decreasing. The threshold depth marked a local maximum in PP and depended on the Z_{Fe} mode. Situations with 250m < Z_{Fe}< 350m corresponded to a transition regime between these two modes, characterized by the presence of two Z_{PPmax} (dashed white lines in Fig. 2a).

The deep iron reservoir mode presented a relatively shallow Z_{PPmax}, at around 200 m. In this mode, iron supplies were systemically low (<10 μmolFe m^{-2} yr^{-1}; black contours in Fig 2a), even when MLD_{winter} was deeper than Z_{Fe} since on those occasions there was only a brief period where MLD was deeper than Z_{Fe}. In contrast, the shallow Z_{Fe} mode was characterized by relatively large iron supplies, which were proportional to MLD_{winter}. In this mode, the threshold depths were deeper (between 350m and 500m) and depended strongly on Z_{Fe}.

In both modes, the iron supply and the contribution of the large phytoplankton group to total PP responded monotonically to changes in MLD_{winter}. This highlights that, as for the example shown in Fig. 1, the threshold depth of MLD_{winter} marks a boundary between two different community responses: for MLD_{winter} shallower than Z_{PPmax}, the community is dominated by small-phytoplankton, and PP of both large and small phytoplankton groups respond monotonically to changes in iron supply (Fig 2b-c); for MLD_{winter} deeper than Z_{PPmax}, the community is dominated

by large-phytoplankton, and light becomes the dominant limiting factor, particularly for the small-phytoplankton group (Fig 2b).

The role of zooplankton in these responses was also addressed by diagnosing the percentage of PP grazed, hereinafter referred as the grazing efficiency. Our simulations show that grazing efficiency was strongly dependent on the community structure (Fig 2d), as small phytoplankton is more easily grazed than large phytoplankton. Such dependency suggests a minor role of zooplankton grazing as it follows the change on community structure, which is in turn caused by changes in MLD.

A further climate-relevant metric associated with marine production is how much of the organic carbon synthetized in the upper ocean is exported to the deep ocean. Under shallow ferricline conditions, the amount of production exported below 100m (EP) showed a non-monotonic response to changing MLD_{winter} with a threshold depth at 500m (Fig. 3a). EP responded in parallel to the productivity supported by the larger class of phytoplankton (Fig. 2c) because large phytoplankton tends to aggregate and sink faster than small phytoplankton (Boyd and Trull, 2007; Laufkötter et al, 2016). In contrast, and unlike PP, under deep ferricline and small phytoplankton conditions we observed a monotonic response, with a constant increase in export as MLD_{winter} decreased (Fig 3a).

4.2 Response to changes in Summer MLD

Phytoplankton growth and primary production rates are the highest during late spring and early summer as surface waters are replenished with iron and light is abundant (Boyd et al 2010). Therefore changes in MLD_{summer}, even if small in magnitude, have the potential to influence annual productivity (Laufkötter et al, 2015; Leung et al, 2015) and export (Hauck et al, 2015). In order to understand the mechanisms by which changes in MLD_{summer} affect primary production, we first compared three simulations with different values of MLD_{summer} (20, 50 and 80 meters) but with, Z_{Fe} set to 150 meters and MLD_{winter} at 300m (Fig 1e). Dissolved iron supplies were very similar among the three simulations but PAR_{ML} strongly differed, with values nine times larger in the shallow experiment than in the deep one (Fig 1f). Stronger light limitation in the deep experiment caused the bloom to be slightly weaker and last longer than in the shallow experiment (Fig 1g). However, annual primary production was the largest in the deep experiment

and this mainly resulted from an increase of the productive volume which caused higher depth-integrated primary production during summer (Fig 1h), despite having the lowest MLD-averaged production rates, PP_{ML} (dashed lines in Fig 1h).

The decrease in annual primary production under shallower MLD_{summer} was consistent amongst all 752 simulations (Fig. 2e). This response suggested that in our model annual primary production was not light limited in summer. MLD_{summer} was always shallower than ferricline depths and iron supply remained low for all scenarios (black lines in Fig 2 e, f, g). Export production was less sensitive to changes in MLD_{summer} than primary production (Fig. 3b), due to the larger contribution of small phytoplankton cells to productivity under deep MLD_{summer} (Fig. 2f).

5 Discussion and Conclusions

The analysis of our ensemble of model simulations revealed that changes in primary production driven by changes in mixed-layer depth are more complex than previously thought. The change in primary production in response to variations in winter mixed-layer was non-monotonous: total primary production and winter mixed-layer depth were positively correlated for winter mixed-layer depths above a certain threshold depth (that we refer as Z_{PPmax}), but negatively correlated for winter mixed-layer depths below this threshold (Fig 2a). The Z_{PPmax} for the mixed-layer emerged due to the overlap of the two limiting factors, light and iron availability (Fig 1b). Interestingly, Z_{PPmax} was related to both the biogeochemical conditions and ecosystem composition. For instance, Z_{PPmax} was shallower for iron-poor and small-phytoplankton dominated conditions than for iron-rich conditions where the two phytoplankton groups contributed more equally (Fig 2b). Our analysis also shown that, quite unexpectedly, deeper summer mixed-layers induced larger total primary production, despite lower phytoplankton growth rates, because of an increase in the productive water volume (Fig 1, right panels and Fig 2a). Lastly, our experiments contribute to an understanding of how changes in MLD can alter the carbon export. As expected, phytoplankton size composition was crucial to controlling carbon export (Fig 3a and b). Under conditions of deep winter mixed-layers and iron-rich environments, decreasing the mixed-layer depth resulted in a reduction of the export by decreasing iron-supply and the presence of fast-sinking large phytoplankton. However, this trend reversed within

environments dominated by small-phytoplankton and export increased with decreasing mixed-layers. Two combined mechanisms likely controlled this trend. In the first place, a larger portion of primary production was grazed by zooplankton (Fig 2d), hence more organic matter could be exported as sinking particles in form of fecal pellets. In the second place, the shallower the mixed-layer the easier for particles to escape from surface turbulence and sink into the ocean (Pavelsky and Doney, 2018).

These results have consequences on how we understand current and future Southern Ocean productivity and export. Firstly, because the iron distribution and winter mixed-layer in the Southern Ocean are zonally asymmetric (Tagliabue et al, 2014), future trends in primary production and export are also likely to vary in both latitude and longitude. This conclusion agrees with the observed zonal asymmetries of phytoplankton phenology provinces (Ardyna et al, 2017) and challenges the prevailing latitudinal pattern of primary production trends projected by most CMIP5 models (Bopp et al, 2013, Leung et al, 2015). We conclude that the latter is more likely to be caused by the inability of current climate models to correctly reproduce the zonal asymmetries in MLD (Sallée et al, 2013) and iron distribution (Schourup-Kristensen, 2015, Tagliabue et al, 2016). Secondly, the non-monotonic response of primary production to MLD should be further explored, particularly in observations, in order to evaluate the threshold depth in winter mixed-layer depth within contrasted bioregions and identify which ecosystems are closer to collapse. Along this line, Ardyna et al. (2017) estimated an average threshold depth over the whole Southern Ocean of ~150m (their Fig S2) that can be used as a benchmark for future studies. From a modeling perspective, evaluating the evolution of trends by decade, instead of just comparing two extreme decades (i.e. projected against historical) may help elucidate the non-monotonic responses in CMIP projections. Lastly, summer results suggest that changes in summer mixed-layer depth do not significantly affect iron supply because the ferricline depth is always deeper than the deepest plausible range of climatological summer mixed-layer depth (see Fig 1c in Tagliabue et al, 2014, which shows that the ferricline depth is deeper than 200m over 75% of the observed summer iron profiles). Summer storms, however, which have not been accounted for in this study, may be more effective in supplying iron in the case of deeper summer mixed-layer depths (Carranza and Gille, 2015, Nicholson et al., 2016).

There are a number of assumptions in our modeling approach that should be kept in mind for future comparisons against observations or more complex models. First, we did not account for silicate limitation. The latter is the main limiting factor for diatoms during late summer in Sub-Antarctic waters of the Southern Ocean (Leblanc et al, 2005). Changes in summer MLD might have a role on re-supplying silicate and alter diatoms summer production. Second, the biogeochemical model used here simulates iron remineralization in a simplistic way (Amount and Bopp, 2006). In our analysis we did not detect any significant change in summer iron concentration associated to remineralization. But it is possible that the representation of this mechanism in our model is too simplistic, because remineralization has been identified as a significant source of iron during summer in the Southern Ocean (Tagliabue et al, 2014 and 2017). How changes in summer mixed-layer depth influence remineralization is out of scope of the current study but together with silicate limitation, these mechanisms could either compensate or intensify the summer trends presented here. Third, we made the choice to not consider changes in incoming solar radiation, and used clear-sky conditions at 45°S latitude in all our experiments. At higher latitudes, where incoming solar radiation is lower, we would expect to find shallower threshold depths, although this could be compensated by higher iron demand by phytoplankton. More difficult is to anticipate the impacts of a non-clear-sky over phytoplankton growth, as incoming solar radiation is simultaneously influenced by seasonal and intra-seasonal variability of cloud coverage, typology of clouds (type and altitude in the atmosphere) and sea-state (surface waves and bubbles). Fourth, we considered changes in MLD but we did not take into account the associated changes in temperature and wind stress. The former is particularly interesting, as laboratory experiments have recently shown interactive effects between iron and temperature for Southern Ocean diatoms (Hutchins and Boyd, 2016). Last, our study is based on a biogeochemical model that, despite its complexity, remains a simplification of the processes regulating phytoplankton growth. For instance, community structure was only represented in terms of size but it is well known that different phytoplankton species of similar sizes respond differently to environmental changes (Arrigo et al., 1999). Also, our model did not account for the potential contribution of vertically migrating zooplankton and small nekton to the carbon export. We should note however that, despite these assumptions, the relationships between primary production and MLD that came out of this modeling study are consistent with that

suggested from in-situ observations (Ardyna et al 2017, Hoppe et al 2017). Moreover, the analysis of a large ensemble of simulations also supports the robustness of our conclusions.

In conclusion, the results presented here provide a new and more refined explanation of the influence of MLD over Southern Ocean primary production and export. They provide a framework to analyze current and future patterns of production and export, in particular for CMIP6 projections and multiannual time-series obtained from *in-situ* observations such as moorings or BGC-Argo floats.

Acknowledgments

We thank Laurent Bopp, Christian Ethé, Julien LeSommer and Olivier Aumont for the technical support and insightful comments that strongly benefited this study. We also thank the two anonymous reviewers who took the time to review this work. We would like to acknowledge support from Sorbonne Université through the project PERSU. This study also benefited from the staff-exchange project SOCCLI, funded by EU (FP7-PEOPLE-2012-IRSES) and the SOBUMS project, funded by the Agence Nationale de la Recherche (ANR-16-CE01-0014). The ensemble of model outputs used in this study can be freely accessed at: https://metadata.imas.utas.edu.au/geonetwork/srv/eng/main.home ; and the PISCES code specific for the model configuration used in this study is available at https://github.com/jllort.

References

Ardyna, M., Claustre, H., Sallée, J.-B., D'Ovidio, F., Gentili, B., van Dijken, G., et al., 2017. Delineating environmental control of phytoplankton biomass and phenology in the Southern Ocean: Phytoplankton Dynamics in the SO. Geophysical Research Letters 44, 5016–5024. https://doi.org/10.1002/2016GL072428

Arrigo, K.R., Robinson, D.H., Worthen, D.L., Dunbar, R.B., DiTullio, G.R., VanWoert, M., Lizotte, M.P., 1999. Phytoplankton Community Structure and the Drawdown of Nutrients and CO2 in the Southern Ocean. *Science* 283 (5400): 365–67. https://doi.org/10.1126/science.283.5400.365.

Aumont, O., Bopp, L., 2006. Globalizing Results from Ocean in Situ Iron Fertilization Studies, *Global Biogeochemical Cycles* 20 (2), 20-2, https://doi.org/10.1029/2005GB002591.

Bissinger, J.E., Montagnes, D.J.S., Harples, J., Atkinson, D., 2008. Predicting marine phytoplankton maximum growth rates from temperature: Improving on the Eppley curve using quantile regression. Limnol. Oceanogr. 53, 487–493. https://doi.org/10.4319/lo.2008.53.2.0487

Bopp, L., Resplandy, L., Orr, J.C., Doney, S.C., Dunne, J.P., Gehlen, M., et al., 2013. Multiple stressors of ocean ecosystems in the 21st century: projections with CMIP5 models. Biogeosciences 10, 6225–6245. https://doi.org/10.5194/bg-10-6225-2013

Boyd, P.W., Strzepek, R., Fu, F., Hutchins, D.A., 2010. Environmental control of open-ocean phytoplankton groups: Now and in the future. Limnology and Oceanography 55, 1353–1376. https://doi.org/10.4319/lo.2010.55.3.1353

Boyd, P.W., Trull, T.W., 2007. Understanding the export of biogenic particles in oceanic waters: Is there consensus? Progress in Oceanography 72, 276–312. https://doi.org/10.1016/j.pocean.2006.10.007

Bracegirdle, T.J., Shuckburgh, E., Sallée, J.B., Wang, Z., Meijers, A. J. S., Bruneau, N., et al., 2013: Assessment of surface winds over the Atlantic, Indian and Pacific Ocean sectors of the Southern Hemisphere in CMIP5 models: historical bias, forcing response, and state dependence,

Journal of Geophysical Research - Atmospheres, 118, 547–562, https://doi.org/10.1002/jgrd.50153

Cai, W., Shi, G., Cowan, T., Bi, D., Ribbe, J., 2005. The response of the Southern Annular Mode, the East Australian Current, and the southern mid-latitude ocean circulation to global warming. Geophysical Research Letters 32. https://doi.org/10.1029/2005GL024701

Cisewski, B., Volker, H. S., and Hartmut, P. 2005. Upper-Ocean Vertical Mixing in the Antarctic Polar Front Zone. *Deep Sea Research Part II: Topical Studies in Oceanography*, Observations and modelling of mixed layer turbulence: Do they represent the same statistical quantities?, 52 (9): 1087–1108. https://doi.org/10.1016/j.dsr2.2005.01.010.

Deppeler, S.L., Davidson, A.T., 2017. Southern Ocean Phytoplankton in a Changing Climate. Front. Mar. Sci. 4. https://doi.org/10.3389/fmars.2017.00040

Doney, S.C., 2006. Oceanography: Plankton in a warmer world. Nature 444, 695–696. https://doi.org/10.1038/444695a

D'Ortenzio, F., Antoine, D., Martinez, E., Ribera d'Alcalà, M., 2012. Phenological changes of oceanic phytoplankton in the 1980s and 2000s as revealed by remotely sensed ocean-color observations, Global Biogeochemical Cycles 26, n/a-n/a. https://doi.org/10.1029/2011GB004269

Eppley, R.W., 1972. Temperature and phytoplankton growth in the sea. Fishery Bulletin 70.

Hauck, J., C. Völker, D. A. Wolf-Gladrow, C. Laufkötter, M. Vogt, O. Aumont, L. Bopp, et al. 2015. On the Southern Ocean CO2 Uptake and the Role of the Biological Carbon Pump in the 21st Century. *Global Biogeochemical Cycles* 29 (9): 1451–70. https://doi.org/10.1002/2015GB005140.

Henson, S. A., Sarmiento, J. L. , Dunne, J. P., Bopp, L. , Lima, I., Doney, S. C. , John, J. and Beaulieu, C. 2010. Detection of Anthropogenic Climate Change in Satellite Records of Ocean Chlorophyll and Productivity, *Biogeosciences* 7 (2): 621–40. https://doi.org/10.5194/bg-7-621-2010.

437 Henson, S.A., Yool, A., Sanders, R., 2015. Variability in efficiency of particulate organic carbon
438 export: A model study, Global Biogeochemical Cycles 29, 33–45.
439 https://doi.org/10.1002/2014GB004965

440 Hoppe, C.J.M., Klaas, C., Ossebaar, S., Soppa, M.A., Cheah, W., Laglera, L.M., et al., 2017.
441 Controls of primary production in two phytoplankton blooms in the Antarctic Circumpolar
442 Current., Deep Sea Research Part II: Topical Studies in Oceanography.
443 https://doi.org/10.1016/j.dsr2.2015.10.005

444 Hutchins, D. A., and P. W. Boyd. 2016. Marine Phytoplankton and the Changing Ocean Iron
445 Cycle. *Nature Climate Change* 6 (12): 1072–79. https://doi.org/10.1038/nclimate3147.

446 Jeandel, C, Ruiz-Pino, D., Gjata, E., Poisson, A., Brunet, C., Charriaud, E., et al., 1998.
447 KERFIX, a Time-Series Station in the Southern Ocean: A Presentation. *Journal of Marine*
448 *Systems* 17 (1–4): 555–69. https://doi.org/10.1016/S0924-7963(98)00064-5.

449 Laufkötter, C., Vogt, M., Gruber, N., Aita-Noguchi, M., Aumont, O., Bopp, L., et al., 2015.
450 Drivers and uncertainties of future global marine primary production in marine ecosystem
451 models. Biogeosciences 12, 6955–6984. https://doi.org/10.5194/bg-12-6955-2015

452 Laufkötter, C., Vogt, M., Gruber, N., Aumont, O., Bopp, L., Doney, S.C., et al., 2016. Projected
453 decreases in future marine export production: the role of the carbon flux through the upper ocean
454 ecosystem. Biogeosciences 13, 4023–4047. https://doi.org/10.5194/bg-13-4023-2016

455 Lenton, A., Matear, R.J., 2007. Role of the Southern Annular Mode (SAM) in Southern Ocean
456 CO_2 uptake. Global Biogeochemical Cycles 21, GB2016. https://doi.org/10.1029/2006GB002714

457 Leung, S., Cabré, A., Marinov, I., 2015. A latitudinally banded phytoplankton response to 21st
458 century climate change in the Southern Ocean across the CMIP5 model suite. Biogeosciences 12,
459 5715–5734. https://doi.org/10.5194/bg-12-5715-2015

460 Lévy, Marina. 2015. Exploration of the Critical Depth Hypothesis with a Simple NPZ Model.
461 *ICES Journal of Marine Science* 72 (6): 1916–25. https://doi.org/10.1093/icesjms/fsv016.

462 Llort, J., Lévy, M., Sallée, J.-B., Tagliabue, A., 2015. Onset, intensification, and decline of
463 phytoplankton blooms in the Southern Ocean. ICES Journal of Marine Science: Journal du
464 Conseil 72, 1971–1984. https://doi.org/10.1093/icesjms/fsv053

465 Lovenduski, N.S., Gruber, N., n.d. Impact of the Southern Annular Mode on Southern Ocean
466 circulation and biology. Geophysical Research Letters 32. https://doi.org/10.1029/2005GL022727

467 Nicholson, S.-A., Lévy, M., Llort, J., Swart, S., Monteiro, P.M.S., 2016. Investigation into the
468 impact of storms on sustaining summer primary productivity in the Sub-Antarctic Ocean.
469 Geophys. Res. Lett. 2016GL069973. https://doi.org/10.1002/2016GL069973

470 Panassa, E., C. Völker, D. Wolf-Gladrow, and J. Hauck. 2018. Drivers of Interannual Variability
471 of Summer Mixed Layer Depth in the Southern Ocean Between 2002 and 2011 *Journal of*
472 *Geophysical Research: Oceans* 123 (8): 5077–90. https://doi.org/10.1029/2018JC013901.

473 Pellichero, V., Sallée, J.-B., Schmidtko, S., Roquet, F., Charrassin, J.-B., 2017. The ocean mixed
474 layer under Southern Ocean sea-ice: Seasonal cycle and forcing. Journal of Geophysical
475 Research: Oceans 122, 1608–1633. https://doi.org/10.1002/2016JC011970

476 Sallée, J.B., Shuckburgh, E., Bruneau, N., Meijers, A.J.S., Bracegirdle, T.J., Wang, Z., 2013.
477 Assessment of Southern Ocean mixed-layer depths in CMIP5 models: Historical bias and forcing
478 response. Journal of Geophysical Research: Oceans 118, 1845–1862.
479 https://doi.org/10.1002/jgrc.20157

480 Sallée, J.B., Speer, K.G., Rintoul, S.R., 2010. Zonally asymmetric response of the Southern
481 Ocean mixed-layer depth to the Southern Annular Mode. Nature Geoscience 3, 273–279.
482 https://doi.org/10.1038/ngeo812

483 Sarmiento, J. L., R. Slater, R. Barber, L. Bopp, S. C. Doney, A. C. Hirst, J. Kleypas, et al. 2004.
484 Response of Ocean Ecosystems to Climate Warming. *Global Biogeochemical Cycles* 18 (3):
485 GB3003. https://doi.org/10.1029/2003GB002134.

486 Schourup-Kristensen, V., 2015. Iron in the Southern Ocean: Spatial distribution and the effect on
487 the phytoplankton. Bremen University, Alfred-Wegener-Institute. http://epic.awi.de/38667/

Siegel, D.A., Behrenfeld, M.J., Maritorena, S., McClain, C.R., Antoine, D., Bailey, S.W., et al., 2013. Regional to global assessments of phytoplankton dynamics from the SeaWiFS mission. Remote Sensing of Environment 135, 77–91. https://doi.org/10.1016/j.rse.2013.03.025

Swart, N.C., Fyfe, J.C., Gillett, N., Marshall, G.J., 2015. Comparing Trends in the Southern Annular Mode and Surface Westerly Jet. J. Climate 28, 8840–8859. https://doi.org/10.1175/JCLI-D-15-0334.1

Swart, N.C., Gille, S.T., Fyfe, J.C. and Gillett, N.P. 2018. Recent Southern Ocean Warming and Freshening Driven by Greenhouse Gas Emissions and Ozone Depletion. *Nature Geoscience* 11 (11): 836. https://doi.org/10.1038/s41561-018-0226-1.

Tagliabue, A., Bowie, A.R., Boyd, P.W., Buck, K.N., Johnson, K.S., Saito, M.A., 2017. The integral role of iron in ocean biogeochemistry. Nature 543, 51–59. https://doi.org/10.1038/nature21058

Tagliabue, A., T. Mtshali, O. Aumont, A. R. Bowie, M. B. Klunder, A. N. Roychoudhury, and S. Swart. 2012. A Global Compilation of Dissolved Iron Measurements: Focus on Distributions and Processes in the Southern Ocean, *Biogeosciences* 9 (6): 2333–49. https://doi.org/10.5194/bg-9-2333-2012.

Tagliabue, A., Sallée, J.-B., Bowie, A.R., Lévy, M., Swart, S., Boyd, P.W., 2014. Surface-water iron supplies in the Southern Ocean sustained by deep winter mixing. Nature Geoscience 7, 314–320. https://doi.org/10.1038/ngeo2101

Takao, S., Hirawake, T., Wright, S.W., Suzuki, K., 2012. Variations of net primary productivity and phytoplankton community composition in the Southern Ocean as estimated from ocean-color remote sensing data. Biogeosciences Discussions 9, 4361–4398. https://doi.org/10.5194/bgd-9-4361-2012

Taylor, K.E., Stouffer, R.J., Meehl, G.A., 2012. An Overview of CMIP5 and the Experiment Design. Bulletin of the American Meteorological Society 93, 485–498. https://doi.org/10.1175/BAMS-D-11-00094.1

513 Zheng, F., Li, J., Clark, R.T., Nnamchi, H.C., 2013. Simulation and Projection of the Southern
514 Hemisphere Annular Mode in CMIP5 Models. Journal of Climate 26, 9860–9879.
515 https://doi.org/10.1175/JCLI-D-13-00204.1
516

FIGURES

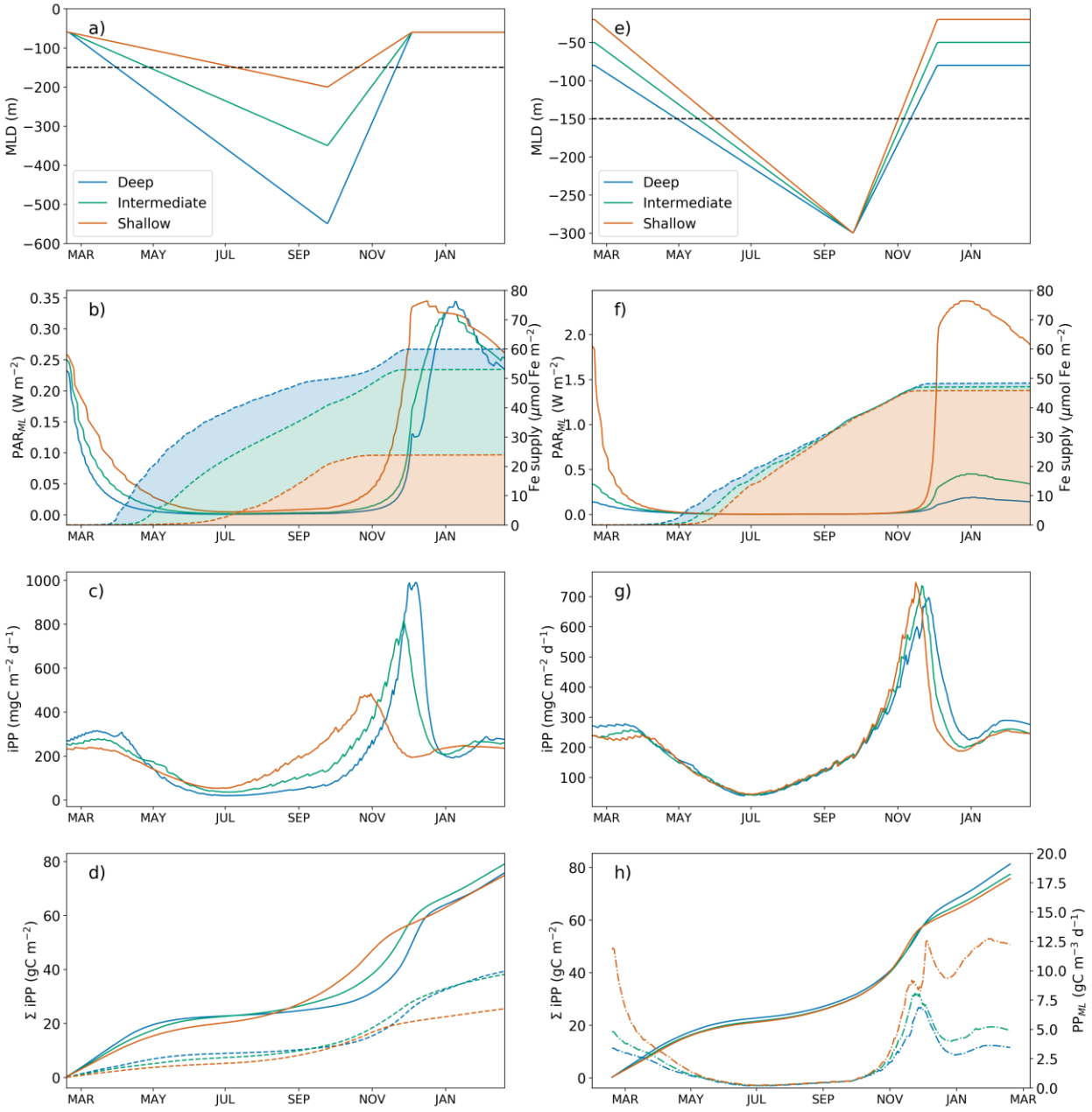
a)
e)
b)
f)
c)
g)
d)
h)
MLD (m)
Deep
Intermediate
Shallow
PAR$_{ML}$ (W m^{-2})
Fe supply (μmol Fe m^{-2})
iPP (mgC m^{-2} d^{-1})
Σ iPP (gC m^{-2})
PP$_{ML}$ (gC m^{-3} d^{-1})
MAR
MAY
JUL
SEP
NOV
JAN

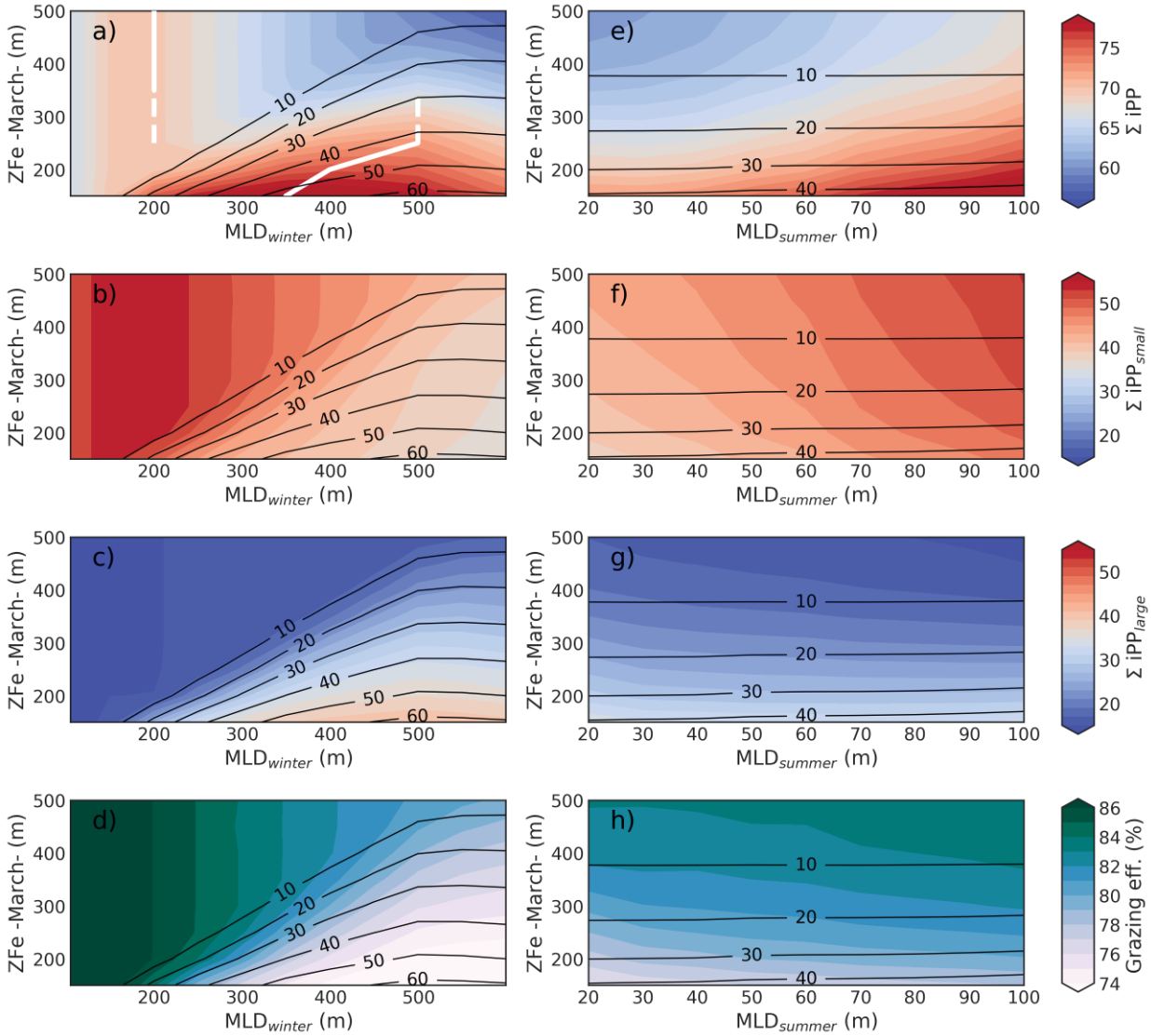
a)
b)
c)
d)
e)
f)
g)
h)
ZFe -March- (m)
MLD$_{winter}$ (m)
MLD$_{summer}$ (m)
Σ iPP
Σ iPP$_{small}$
Σ iPP$_{large}$
Grazing eff. (%)

520

521

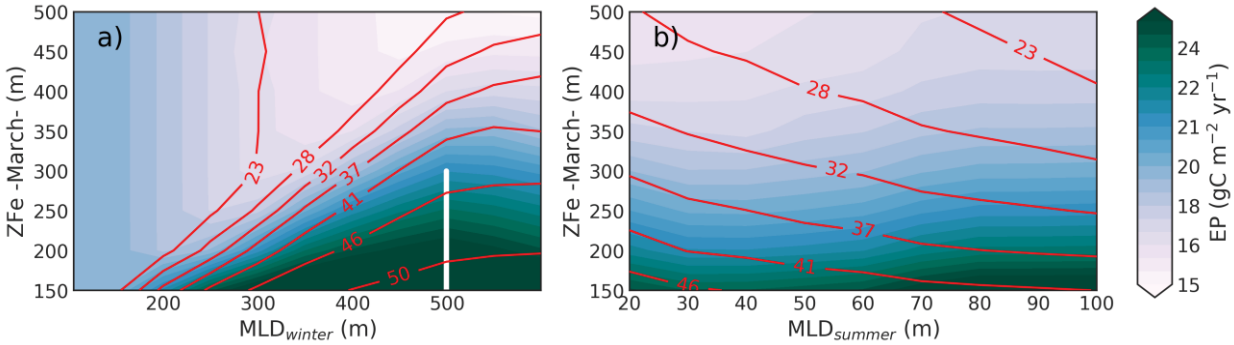
a)
b)
ZFe -March- (m)
MLD$_{winter}$ (m)
MLD$_{summer}$ (m)
EP (gC m^{-2} yr^{-1})
23
28
32
37
41
46
50

522

523

CAPTIONS

Figure 1: *Left panels: Seasonal cycles of (a) mixed layer depth, (b) averaged PAR in the MLD (plain lines) and time-cumulative vertical supply of iron (dashed contours with colors filled) into the MLD, (c) depth-integrated primary production (iPP), and (d) time-cumulative integrated primary production (ΣiPP, plain lines) and integrated primary production for the large-phytoplankton group (dashed lines) for three simulations with identical Z_{Fe} depth and MLD_{summer} but with different MLD_{winter}. The black dashed line in (a) indicates the value of Z_{Fe}. Right panels: same but for simulations runs with identical Z_{Fe} depth and MLD_{winter} and different MLD_{summer}. In h), dash-dotted lines represent primary production averaged in the mixed-layer (PP_{ML}).*

Figure 2: *Left panels: a) Annual integrated Primary Production (in gC m^{-2} yr^{-1}) as a function of initial Ferricline depth (Z_{Fe}) and winter MLD (MLD_{winter}). White solid lines indicate threshold depths (Z_{PPmax}) and white dashed lines indicate the range where two different thresholds were detected. c) Same as a) but for small phytoplankton. c) Same as a) but for large phytoplankton. d) Portion of annual primary production grazed by zooplankton (grazing efficiency). In all panels, the black contours show the vertical supply of iron (nmolFe/yr). Right panels: same, but against summer MLD (MLD_{summer}).*

Figure 3: *a) Annual Primary Production exported below 100m depth as a function of initial Ferricline depth (Z_{Fe}) and winter MLD (MLD_{winter}). Red contours show the percentage of primary production done by the large (and fast-sinking) phytoplankton. The white line indicates the threshold depth for EP-MLD relationship. b) Same as a) but against summer MLD (MLD_{summer}).*

Figure 1.

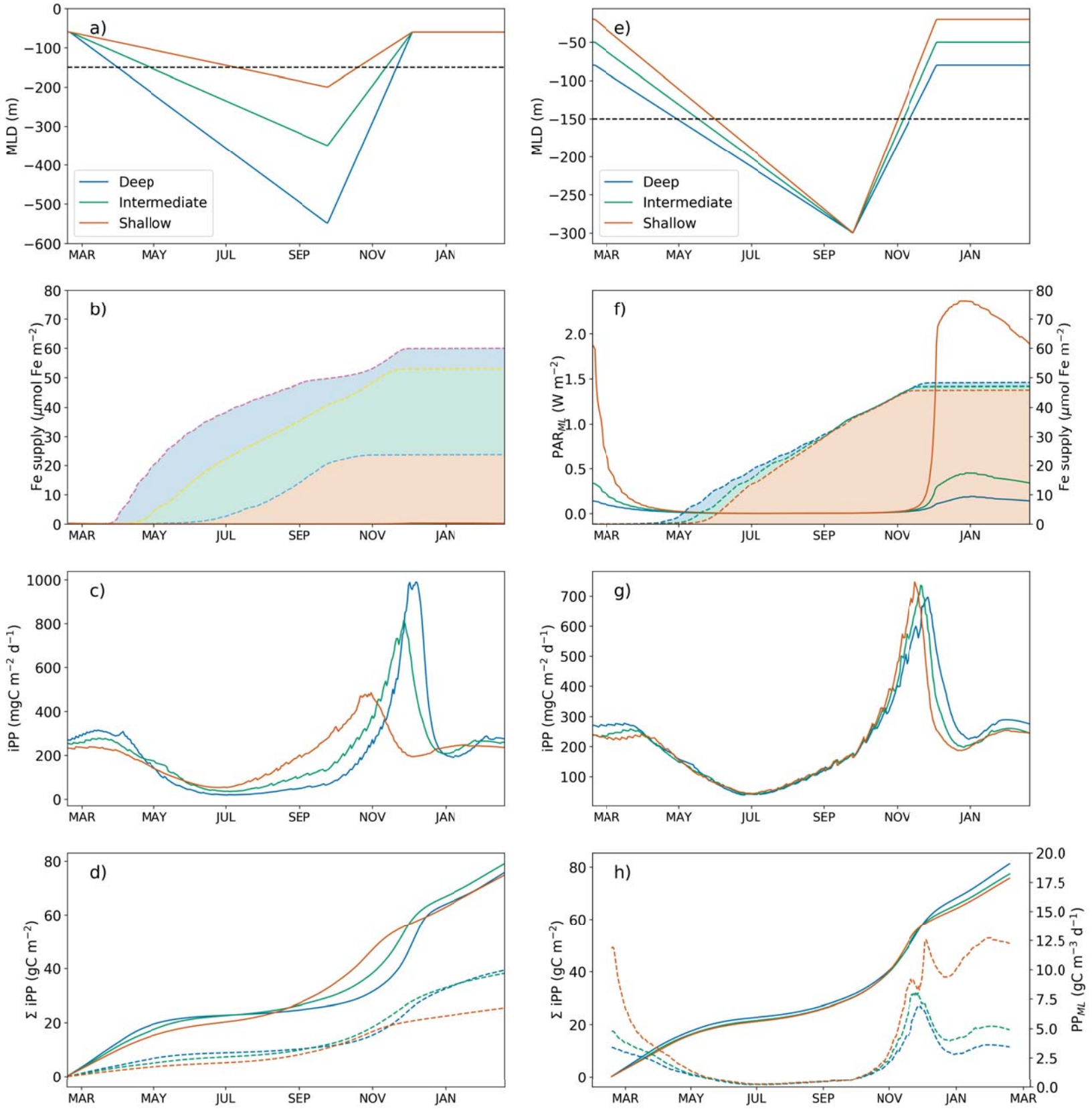
a)
MLD (m)
Deep
Intermediate
Shallow
MAR
MAY
JUL
SEP
NOV
JAN
e)
b)
Fe supply (μmol Fe m⁻²)
f)
PAR_ML (W m⁻²)
c)
iPP (mgC m⁻² d⁻¹)
g)
d)
Σ iPP (gC m⁻²)
h)
PP_ML (gC m⁻³ d⁻¹)

Figure 2.

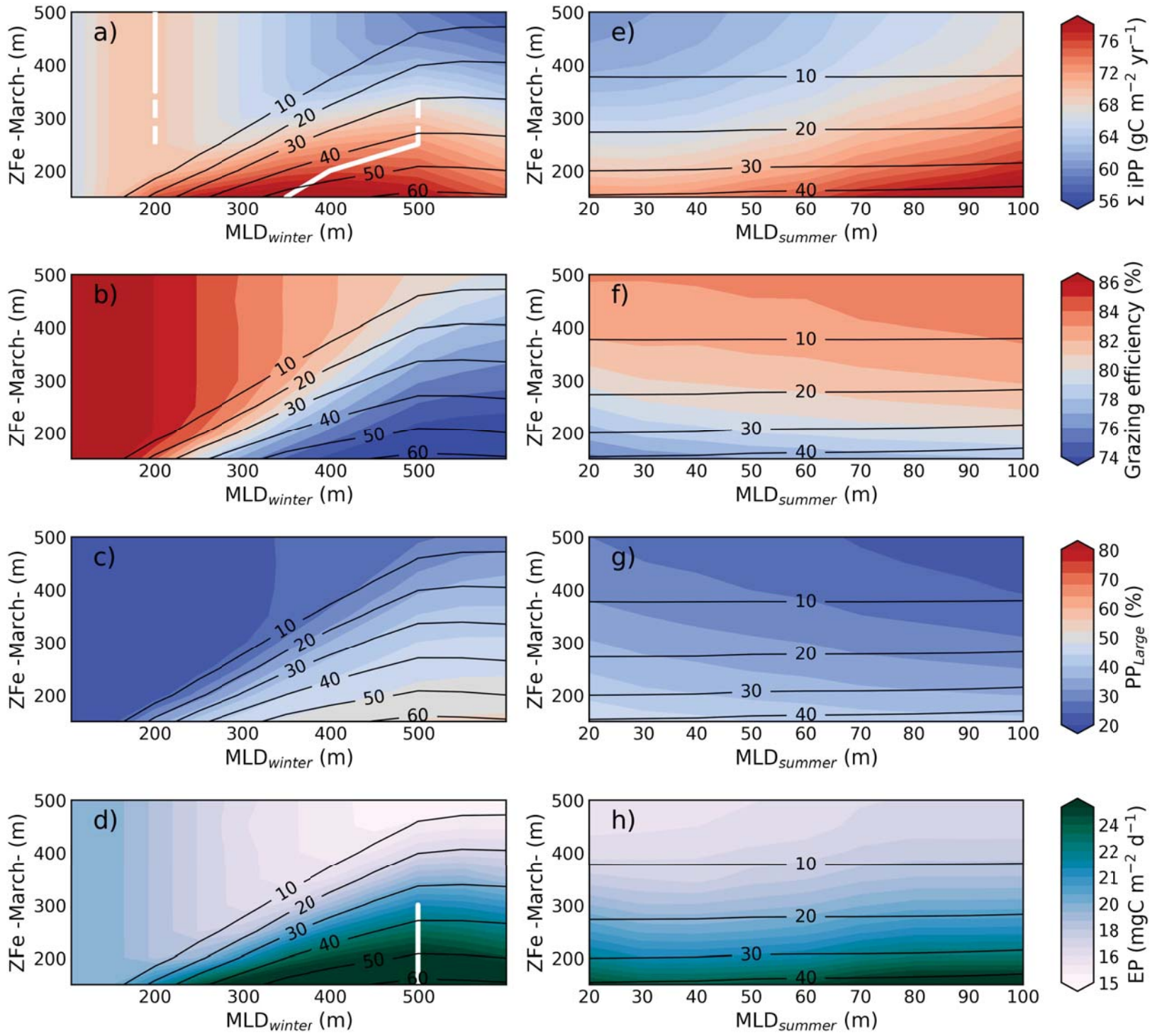
a)
b)
c)
d)
e)
f)
g)
h)
ZFe -March- (m)
MLD$_{winter}$ (m)
MLD$_{summer}$ (m)
Σ iPP (gC m^{-2} yr^{-1})
Grazing efficiency (%)
PP$_{Large}$ (%)
EP (mgC m^{-2} d^{-1})

Figure 3.

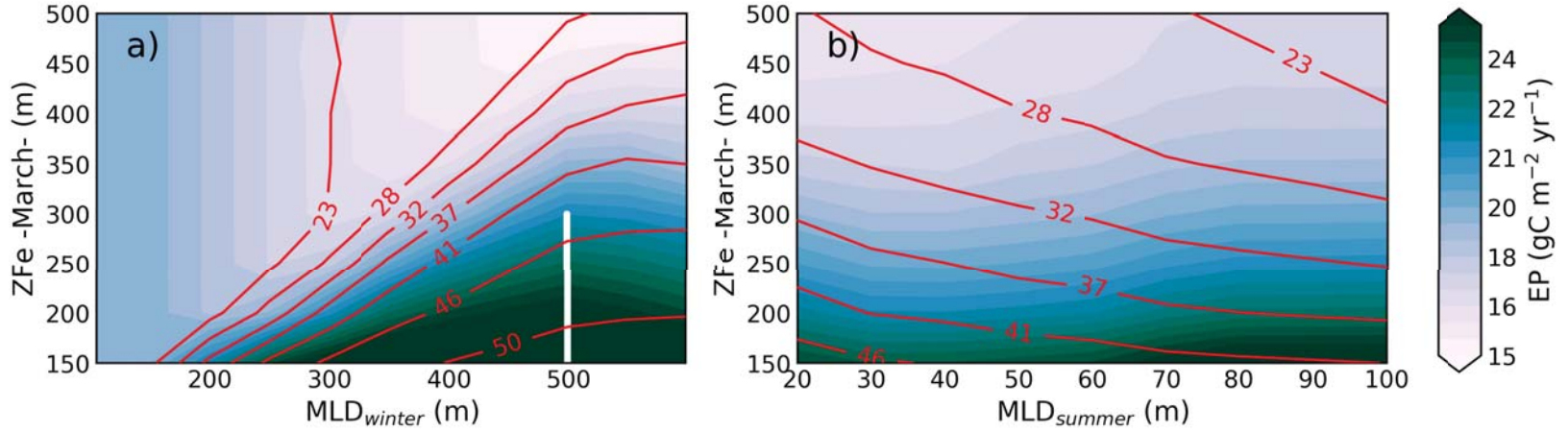
a)
b)
ZFe -March- (m)
MLD$_{winter}$ (m)
MLD$_{summer}$ (m)
EP (gC m^{-2} yr^{-1})
23
28
32
37
41
46
50